

COMPRESSIBLE FLOW IN FRONT OF AN AXISYMMETRIC BLUNT OBJECT: ANALYTIC APPROXIMATION AND ASTROPHYSICAL IMPLICATIONS

URI KESHET AND YOSHI NAOR

Physics Department, Ben-Gurion University of the Negev, PO Box 653, Be'er-Sheva 84105, Israel; ukeshet@bgu.ac.il

Draft version November 22, 2016

ABSTRACT

Compressible flows around blunt objects have diverse applications, but current analytic treatments are inaccurate and limited to narrow parameter regimes. We show that the gas-dynamic flow in front of an axisymmetric blunt body is accurately derived analytically using a low order expansion of the perpendicular gradients in terms of the parallel velocity. This reproduces both subsonic and supersonic flows measured and simulated for a sphere, including the transonic regime and the bow shock properties. Some astrophysical implications are outlined, in particular for planets in the solar wind and for clumps and bubbles in the intergalactic medium. The bow shock standoff distance normalized by the obstacle curvature is $\sim 2/(3g)$ in the strong shock limit, where g is the compression ratio. For a subsonic Mach number M approaching unity, the thickness δ of an initially weak, draped magnetic layer is a few times larger than in the incompressible limit, with amplification $\sim (1 + 1.3M^{2.6})/(3\delta)$.

Subject headings: hydrodynamics – shock waves – methods: analytical – intergalactic medium – interplanetary medium

1. INTRODUCTION

Compressible flows around blunt objects play an important role in diverse fields of science and engineering, ranging from fluid mechanics (*e.g.*, Landau & Lifshitz 1959; Park et al. 2006; Mack & Schmid 2011; Tutty et al. 2013; Grandemange et al. 2013, 2014), space physics (*e.g.*, Spreiter & Alksne 1970; Baranov & Lebedev 1988; Spreiter & Stahara 1995; Cairns & Grabbe 1994; Petrincic & Russell 1997; Petrincic 2002), and astrophysics (Lea & De Young 1976; Shaviv & Salpeter 1982; Canto & Raga 1998; Schulreich & Breitschwerdt 2011), to computational physics and applied mathematics (Hejranfar et al. 2009; Wilson 2013; Gollan & Jacobs 2013; Marrone et al. 2013), aeronautical and civil engineering (Nakanishi & Kamemoto 1993; Baker 2010; Aul'chenko et al. 2012), and aerodynamics (Asanaliev et al. 1988; Liou & Takayama 2005; Pilyugin & Khlebnikov 2006; Volkov 2009). Yet, even for the simple case of an inviscid flow around a sphere, the problem has resisted a general or accurate analytic treatment due to its nonlinear nature.

In particular, in space physics and astrophysics, the interaction of an ambient medium with much denser, in comparison approximately solid, bodies such as comets (*e.g.*, Baranov & Lebedev 1988), planets (Spreiter & Alksne 1970; Cairns & Grabbe 1994; Petrincic & Russell 1997), binary companions (Canto & Raga 1998), galaxies (Shaviv & Salpeter 1982; Schulreich & Breitschwerdt 2011), or large scale clumps and bubbles (Lea & De Young 1976; Vikhlinin et al. 2001; Lyutikov 2006; Markevitch & Vikhlinin 2007), is important for modeling these systems and understanding their observational signature. This is particularly true for the shocks formed in supersonic flows, due to their rich nonthermal effects (*e.g.*, Spreiter & Stahara 1995; Vikhlinin et al. 2001; Petrincic 2002; Markevitch & Vikhlinin 2007).

Although these fairly complicated systems can be approximately solved numerically, they are often modeled as an idealized, inviscid flow around a simple blunt object, often approximated as axisymmetric or even spherical, with some simplified analytic description employed in order to gain a deeper, more general understanding of the system. Consequently, this fundamental problem of fluid mechanics has received considerable attention. The small Mach number M regime was studied as an asymptotic series about $M = 0$ (Lord Rayleigh 1916; Tamada 1939; Kaplan 1940; Stangeby & Allen 1971; Allen 2013), and solved in the incompressible potential flow limit. Some hodograph plane results and series approximations were found in the transonic and supersonic cases (Hida 1955; Liepmann & Roshko 1957; Guderley 1962). In particular, approximations for the standoff distance of the bow shock (*e.g.*, Moeckel 1949; Hida 1953; Lighthill 1957; Hayes & Probstein 1966; Spreiter et al. 1966; Guy 1974; Corona-Romero & Gonzalez-Esparza 2013) partly agree with experiments (*e.g.*, Heberle et al. 1950; Schwartz & Eckerman 1956), spacecraft data (Farris & Russell 1994; Spreiter & Stahara 1995; Verigin et al. 1999), and numerical computations (Chapman & Cairns 2003; Igra & Falcovitz 2010).

However, these analytic results are typically based on ad hoc, unjustified assumptions, such as negligible compressibility effects, a predetermined shock geometry (Lighthill 1957; Guy 1974), or an incompressible (Hida 1953) or irrotational (Kawamura 1950; Hida 1955) flow downstream of the shock. Other approaches use slowly converging, or impractically complicated, expansion series (Lord Rayleigh 1916; Hida 1955; Van Dyke 1958a, 1975). In all cases, the results are inaccurate or limited to a narrow parameter regime. A generic yet accurate analytic approach is needed.

We adopt the conventional assumptions of (i) an ideal, polytropic gas with an adiabatic index γ ; (ii) negligible viscosity and heat conduction (ideal fluid); (iii) a steady,

laminar, non-relativistic flow; and (iv) negligible electromagnetic fields. Typically, these assumptions hold in front of the object, but break down behind it and in its close vicinity. We thus analyze the flow ahead of the object.

While spatial series expansions and hodograph plane analyses, when employed separately, are of limited use (for reviews, see [Van Dyke 1958b](#); [Van Dyke 1975](#)), we find that their combination gives good results over the full parameter range. In particular, we expand the axial flow in terms of the parallel velocity, rather than of distance. This yields an accurate, fully analytic description of the gas-dynamic flow, in both subsonic and supersonic regimes, already in a second or third order expansion, as shown in Fig. 1.

After introducing the flow equations in §2, in particular along the axis of symmetry, we derive the expansion series for the subsonic regime in §3, and for the supersonic regime in §4. Some astrophysical implications are demonstrated in §5, in particular for planetary bow shocks and for clumps and bubbles in the intergalactic medium (IGM). We begin the analysis with a sphere, and outline the generalization for arbitrary blunt axisymmetric objects in §6, where the results are summarized and discussed. For convenience, the full results are given explicitly in Appendix §A.

2. FLOW EQUATIONS

Under the above assumptions, the flow is governed by the stationary continuity, Euler, and energy equations,

$$\nabla \cdot (\rho \mathbf{v}) = 0; \quad (\mathbf{v} \cdot \nabla) \mathbf{v} = -\frac{\nabla P}{\rho}; \quad \mathbf{v} \cdot \nabla \left(\frac{P}{\rho^\gamma} \right) = 0, \quad (1)$$

where \mathbf{v} , P and ρ are the velocity, pressure and mass density. At a shock, downstream (subscript d) and upstream (u) quantities are related by the shock adiabat (e.g., [Landau & Lifshitz 1959](#)),

$$\frac{\rho_d}{\rho_u} = \frac{v_u}{v_d} = \frac{(\gamma + 1)M_u^2}{(\gamma - 1)M_u^2 + 2}; \quad \frac{P_d}{P_u} = \frac{2\gamma M_u^2 + 1 - \gamma}{\gamma + 1}, \quad (2)$$

with $M \equiv v/c$, and $c = (\gamma P/\rho)^{1/2}$ being the sound speed.

Along streamlines, Bernoulli's equation implies that

$$w + v^2/2 = \bar{w} = \text{const.}, \quad (3)$$

where $w = \gamma P/[(\gamma - 1)\rho]$ is the enthalpy, and a bar denotes (henceforth) a putative stagnation ($v = 0$) point. The far incident flow is assumed to be uniform and unidirectional, so \bar{w} is the same constant for all streamlines. Equation (3) remains valid across shocks, as $w + v^2/2$ is the ratio between the normal fluxes of energy and of mass, each conserved separately across a shock.

Bernoulli's equation (3) relates the local Mach number,

$$M = v/c = (M_0^{-2} - S^{-2})^{-\frac{1}{2}} = (\Pi^{-\frac{\gamma-1}{\gamma}} - 1)^{\frac{1}{2}} S, \quad (4)$$

to the Mach number with respect to stagnation sound, $M_0 \equiv v/\bar{c}$, and to the normalized pressure, $\Pi \equiv P/\bar{P}$. We define $S^2 \equiv 2/(\gamma - 1)$ and $W^2 \equiv 2/(\gamma + 1)$ as the strong and weak shock limits of M_0^2 , so the subsonic (supersonic) regime becomes $0 < M_0 < W$ ($W < M_0 < S$). Figure 1 illustrates these definitions, and shows the shock adiabat Eq. (2) (as horizontal jumps at fixed r) for $\gamma = 7/5$.

Consider the flow ahead of a sphere along the symmetry axis, $\theta = 0$ in spherical coordinates $\{r, \theta, \phi\}$. Here, the flow monotonically slows with decreasing r , down to $v = 0$ at the stagnation point, which we normalize as $\bar{\mathbf{r}} = \{1, 0, 0\}$. Symmetry implies that along the axis $\mathbf{v} = -u(r)\hat{\mathbf{r}}$, where $u > 0$. Here, Eqs. (1) become

$$\frac{\partial \ln(\rho u)}{\partial \ln r^2} = \frac{q - u}{u}; \quad \partial_r P = -\rho u \partial_r u; \quad \partial_\theta P = 0, \quad (5)$$

along with Bernoulli's Eq. (3), where we defined $q \equiv (\partial_\theta v_\theta)_{\theta=0}$ as a measure of the perpendicular velocity. Hence,

$$\partial_r u = \frac{2}{r}(q - u) \frac{1 - M_0^2/S^2}{1 - M_0^2/W^2}. \quad (6)$$

Our analysis relies on $u(r)$ being a monotonic function. This allows us to write $q = q(u)$ as a function of u and not of r . Integrating Eq. (6) thus yields

$$2 \ln r = \int_0^{u(r)} \frac{1 - M_0(u')^2/W^2}{1 - M_0(u')^2/S^2} \frac{du'}{q(u') - u'}, \quad (7)$$

so given $q(u)$, the near-axis flow is directly determined.

Unlike $u(r)$, or other expansion parameters used previously, the $q(u)$ profile for typical bodies varies little, and nowhere vanishes. It is well approximated by a few terms in a power expansion of the form

$$q(u) = q_0 + q_1(u - U) + q_2(u - U)^2 + \dots, \quad (8)$$

where U is a reference velocity, so the integral in Eq. (7) can be analytically carried out to any order (see §A). Moreover, we next show that the boundary conditions tightly fix $q(u)$, giving a good approximation for the near axial flow.

First expand $q \simeq \bar{q}$ near stagnation, with $U = \bar{u} = 0$. An initially homogeneous subsonic or even mildly supersonic ([Landau & Lifshitz 1959](#)) flow remains irrotational, $\nabla \times \mathbf{v} = 0$, in which case the lowest-order constraint is

$$\bar{q}_1 = -1/2, \quad (9)$$

whereas for a supersonic, rotational flow, it becomes

$$3\bar{c}^2\bar{q}_3 + 7\bar{c}\bar{q}_2 = 2\bar{q}_1 + 6\frac{\bar{q}_0}{\bar{c}} + \bar{q}_1 \left(\frac{\bar{q}_0}{\bar{c}} \right)^2 + \left(\frac{\bar{q}_0}{\bar{c}} \right)^3, \quad (10)$$

as seen by expanding Eqs. (1) to order $\theta^2(r - 1)^3$. The generalization for non-spherical objects is discussed in §6. Next, we estimate q far from the body, and use it to approximate the flow in both the subsonic (§3) and supersonic (§4) regimes.

3. SUBSONIC FLOW

In the subsonic, $\tilde{M} < 1$ case, we derive the incoming axial flow out to $r \rightarrow \infty$. Using the incident flow (labeled by a tilde, henceforth) boundary condition $\tilde{\mathbf{v}} = \tilde{u}\{-\cos\theta, \sin\theta, 0\}$, we may expand \tilde{q} with $U = \tilde{u}$, such that

$$\tilde{q}_0 = (\partial_\theta \tilde{v}_\theta)_{\theta=0} = \tilde{u}. \quad (11)$$

Additional terms can be derived using $\tilde{M} \ll 1$ or $r \gg 1$ expansions appropriate for the relevant object. Here, it

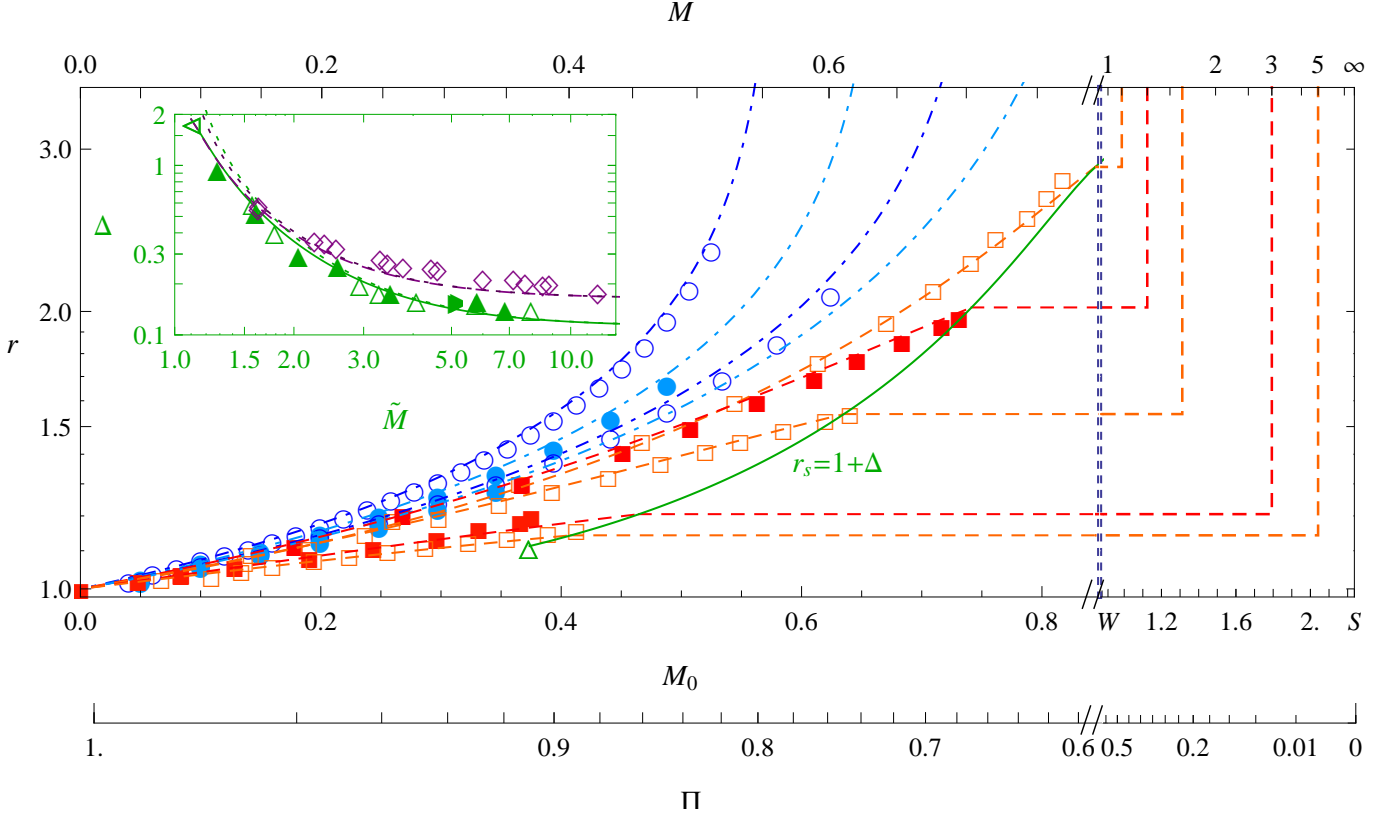


FIG. 1.— Radial profiles of Mach number M (top axis) and of normalized velocity M_0 and pressure Π (bottom axis; see definitions in Eq. 4) in front of a unit ($r = 1$) sphere, for $\gamma = 7/5$, according to numerical simulations (symbols) and our approximation (curves), in both subsonic (bluish circles and dot-dashed curves) and supersonic (reddish squares and dashed curves) regimes. Numerical data shown (alternating shading to guide the eye) for $\tilde{M} = 0.6, 0.7, 0.8, 0.95$ (Karanjkar 2008), 1.1, 1.3, 1.62 (Krause 1975; Heberle et al. 1950), 3 (Bono & Awruch 2008), and 5 (Krause 1975; Sedney & Kahl 1961). The shock standoff distance (solid green) with its $\tilde{M} \rightarrow \infty$ limit (triangle) are also shown. The right side of the figure extends it (on a different scale, to show the full M range) to the supersonic, $M > 1$ part of the flow, upstream of shocks; horizontal jumps represent the shock adiabat Eq. (2). *Inset*: standoff distance measured experimentally (symbols) and using the parameter-free (dotted curves; Eq. (18)) and single-parameter fit (Eq. (19)) approximations, for $\gamma = 7/5$ (triangles; Heberle et al. (1950); Van Dyke (1958b); Sedney & Kahl (1961); Krause (1975); solid curve for $\beta = 0.48$) and $\gamma = 5/3$ (diamonds; Schwartz & Eckerman (1956); dashed curve for $\beta = 0.52$).

will suffice to consider the leading, $(u - \tilde{u}) \propto r^{-\alpha}$ behavior at large radii, such that Eq. (6) yields

$$\tilde{q}_1 = 1 - \frac{\alpha}{2} \frac{1 - \tilde{M}_0^2/W^2}{1 - \tilde{M}_0^2/S^2}. \quad (12)$$

In the incompressible limit, $\alpha = 3$ for any object (e.g., Landau & Lifshitz 1959). This also holds for general forward-backward symmetric objects in any potential flow. To see the latter, expand the potential Φ , defined by $\mathbf{v} = \tilde{\mathbf{u}} \nabla \Phi$, as a power series in r . Imposing the $r \rightarrow \infty$ boundary conditions and regularity across $\theta = 0$ yields

$$\Phi = -r \cos \theta + \frac{\varphi_1}{r\Theta} + \frac{\varphi_2 \cos \theta}{r^2 \Theta^3} + \dots, \quad (13)$$

where $\Theta \equiv [1 - M^2(S^{-2} + \sin^2 \theta)]^{1/2}$. The constants φ_k are determined by the boundary conditions on the specific body. Symmetry under forward-backward inversion, $\Phi \rightarrow -\Phi$ if $\theta \rightarrow \pi - \theta$, requires that $\varphi_1 = 0$. In general $\varphi_2 \neq 0$, implying that indeed $\alpha = 3$. Such behavior is demonstrated for an arbitrary compressible flow around a sphere by the Janzen-Rayleigh series (e.g., Tamada 1939; Kaplan 1940).

Finally, the \tilde{q} expansion at $r \rightarrow \infty$ is matched to the

\tilde{q} expansion at stagnation for a potential flow. In the limit of an incompressible flow around a sphere, Eqs. (9), (11), and (12) yield $q(u) = \tilde{u} - (u - \tilde{u})/2 + O(u - \tilde{u})^2 = 3\tilde{u}/2 - u/2$, which is indeed the exact solution.

This procedure reasonably approximates arbitrary compressible, subsonic flows. Better results are obtained by noting that the constraint (9) holds also before stagnation, as long as $\partial_{\theta\theta} v_r$ is negligible, implying that $\tilde{q}_2 \simeq 0$. Combining this with constraints (9), (11), and (12) yields an accurate, third order approximation, shown in Fig. 1 as dot-dashed curves. See §A.1 for an explicit solution.

4. SUPERSONIC FLOW

In the supersonic, $\tilde{M} > 1$ case, a detached bow shock forms in front of the object, at the so-called standoff distance Δ from its nose. The transition between subsonic and supersonic regimes is continuous, so $\Delta \rightarrow \infty$ as $\tilde{M} \rightarrow 1$, or equivalently as $\tilde{M}_0 \rightarrow W$. The unperturbed upstream flow and the shock transition are shown on the right side of Fig. 1.

Consider the flow between the shock and stagnation along the axis of symmetry. The $q(u)$ profile is strongly constrained if the normalized shock curvature $\xi^{-1} \equiv (R/r_s)_{\theta=0}$ is known. Here, r_s is the shock radius, such that $r_s(\theta = 0) = 1 + \Delta$, and $R = r_s/[1 - r_s''(\theta)/r_s]$ is its

local radius of curvature.

Expanding the flow Eqs. (1) using Eqs. (2) as boundary conditions, yields the $q^{(d)}$ expansion coefficients around $U = u_d$, just downstream of the shock,

$$q_0^{(d)} = (1 + g\xi - \xi) g^{-1} \tilde{u}; \quad (14)$$

$$q_1^{(d)} = \frac{3 + (g-3)\xi}{2} - \frac{1 + (3g-1)\xi}{1 + g + (g-1)\gamma}; \quad (15)$$

and

$$q_2^{(d)} = \frac{g\xi W^2}{8(g+W^2-1)^2 \tilde{u}} \left[\frac{g^2 - 4g + 3}{\xi W^2} - \frac{2(3g+1)}{\xi} \right. \\ \left. + 2(g^2 + 4g + 1) - \frac{(g-1)^2(g+3)}{W^2} + \frac{8g^2 W^2}{g-1} \right], \quad (16)$$

where $g \equiv (\tilde{M}_0/W)^2 \geq 1$ is the axial compression ratio.

These coefficients depend on the shock profile only through ξ ; higher order terms are sensitive to deviations of the profile from a sphere of radius R . In the weak shock limit $g \rightarrow 1$, so ξ must vanish to avoid the divergence of $q_2^{(d)}$. This implies that R diverges faster than Δ , and $q_1^{(d)} \rightarrow (1 - 2\xi)$ asymptotes to unity, consistent with a smooth transition to the subsonic regime. Moreover, if we require that $q_2^{(d)} \rightarrow \tilde{q}_2 \rightarrow 3/(2\tilde{c}W)$ in this limit (see §A.1), then

$$\xi(\tilde{M}_0 \simeq W) \rightarrow (4 + \gamma)(-1 + \tilde{M}_0/W), \quad (17)$$

so R/r_s diverges as $(\tilde{M}_0 - W)^{-1}$, consistent with Hida (1953, 1955, as expected in the irrotational limit).

Equations (14)–(16) yield a good, second order approximation to the flow, as shown in Fig. 1 (dashed curves), once ξ or any of the $q^{(d)}$ coefficients are determined. This can be done using the stagnation boundary conditions, such as Eq. (10), but is laborious and body-specific due to the high order involved. A simpler approach is to estimate $\xi(M)$ using the weak and strong shock limits.

In the strong shock, $\tilde{M}_0 \rightarrow S$ limit, the curvature of the shock approaches that of the object (*e.g.*, Guy 1974); $\xi \rightarrow 1$ in the case of the sphere. The $\tilde{M}_0(\xi)$ relation may be derived as a power series, using this and the constraint Eq. (17). A second order expansion in ξ gives a good approximation, valid throughout the supersonic regime,

$$\frac{\tilde{M}_0}{W} - 1 \simeq \frac{\xi}{4 + \gamma} + \left(\frac{S}{W} - \frac{5 + \gamma}{4 + \gamma} \right) \xi^2, \quad (18)$$

with no free parameters. The good fit suggests that higher order terms in ξ are negligible or absent.

Alternatively, the result $\xi(\tilde{M}_0 \rightarrow S) = 1$ and direct measurements of ξ (Heberle et al. 1950), motivate a power-law approximation of the form

$$\xi \simeq \left[(\tilde{M}_0 - W)/(S - W) \right]^\beta. \quad (19)$$

We find that Eq. (19) nicely fits the measured flow for Mach numbers not too small, with $\beta \simeq 1/2$.

The standoff distance may now be found by solving Eq. (7) for $r_s = 1 + \Delta$, taking $u = u_d$ or equivalently $M_0 = \tilde{M}_0/g = W^2/\tilde{M}_0$, using the expansion (8) with

coefficients (14–16) fixed by the $\xi(\tilde{M}_0)$ relation. The figure inset shows that Eq. (18) provides a good fit to the standoff distance throughout the supersonic range, for two equations of state. It also shows that a single $\beta \simeq 1/2$ power-law in Eq. (19) reproduces Δ away from the transonic regime. Indeed, Δ is sensitive to the precise value of β only in the $M \simeq 1$ limit; best results are obtained with $\beta = 0.48$ ($\beta = 0.52$) for $\gamma = 7/5$ ($\gamma = 5/3$).

5. ASTROPHYSICAL IMPLICATIONS

The above prescription for the flow in front of a blunt object is useful in a wide range of astrophysical circumstances, as the low-density medium can often be approximated as ideal and inviscid, the body as impenetrable, and the motion as steady and non-relativistic.

Consider for example the standoff distance Δ in front of a supersonic astronomical object. It is useful to plot Δ as a function of the compression ratio g , rather than of the Mach number, because it is typically easier to measure g . As Fig. 2 shows, $\Delta(g)$ at a given γ approximately follows a power-law, for example $\Delta(\gamma = 7/5) \simeq 1.6g^{-1.5}$ and $\Delta(\gamma = 5/3) \simeq 1.5g^{-1.6}$. For high \tilde{M} , the standoff distance approaches the strong shock limit, approximately given by (see §A.3.3)

$$\Delta(\tilde{M} \rightarrow \infty) \simeq \frac{2}{3g}. \quad (20)$$

For an arbitrary axisymmetric blunt body, the above results for a sphere are trivially generalized, if Δ is defined as the distance from the nose of the body, normalized by its radius of curvature (for additional corrections, see §6). One may thus superimpose $\Delta(g)$ estimates of astronomical bow shocks on Fig. 2, even for non-spherical bodies.

Consider for example the bow shock of a planet, moving supersonically through the solar wind. Although the magnetic Mach number and the ratio Δ/λ_i (λ_i being the ion gyroradius) are not very high in such systems, a gas-dynamic approach remains useful as a first approximation, provided that \tilde{M} is replaced by the fast magnetosonic Mach number upstream (Stahara 1984; Spreiter & Stahara 1995; Fairfield et al. 2001). Here, we define Δ as the distance between the bow shock and the nose of the obstacle, namely the planetary magnetosphere or ionosphere, normalized by the radius of curvature of this obstacle's nose. For a discussion of planetary bow shocks, and a compilation of Δ estimates based on analytic arguments and numerical simulations, see Verigin et al. (2003, and references therein). Note that our analysis directly provides not only $\Delta(g)$, but also the flow profile and the shock radius of curvature.

Estimates of $\Delta(g)$ for the solar system planets are shown in Fig. 2, with references provided in the caption. Interestingly, some planetary data seem to suggest a soft equation of state with $\gamma < 5/3$. However, such an interpretation is hindered by the substantial simplifying assumptions, in particular the neglected MHD effects, kinetic effects, variable solar wind conditions, and non-axisymmetric corrections to the obstacles. The positions and shapes of the obstacles are in some cases highly uncertain; indeed, the results suggest a significant flattening of the magnetospheres of Saturn and Uranus.

As another astronomical system, consider the large

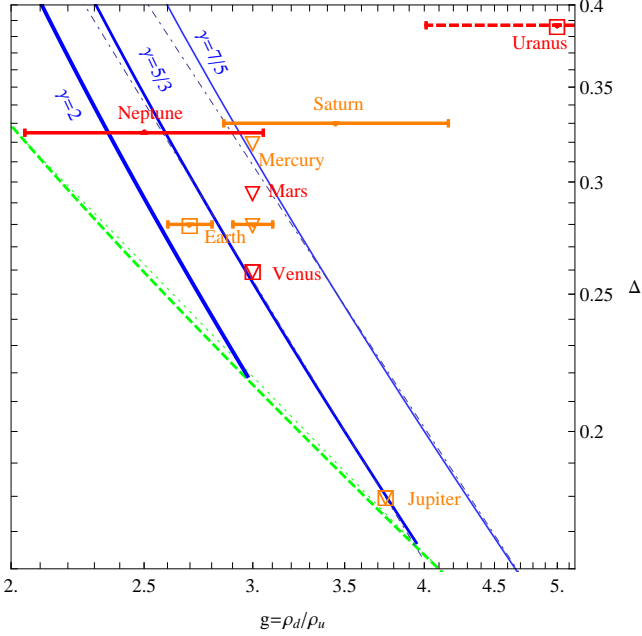


FIG. 2.— Bow shock standoff distance Δ , measured from the nose of the obstacle and normalized by the nose curvature of the obstacle, plotted against the compression ratio g . Analytic curves for $\gamma = 7/5$, $5/3$ and 2 (solid, thin to thick) are shown alongside planet data (labeled symbols), and approximated as power laws (dot-dashed curves, see text). Also plotted is the strong shock limit for various γ (dashed), well fit by $\Delta \sim 2/(3g)$ (dotted). Planetary g values are based on magnetic (triangle) or no symbol (when available) for Mercury (slightly perpendicular shock; measured at $\theta_p \simeq 70^\circ$; Anderson et al. 2008; Treumann & Jaroschek 2008; Slavin et al. 2012), Venus (day side; Treumann & Jaroschek 2008; Frank et al. 1991), Earth (quasi-perpendicular; $\theta_p \lesssim 45^\circ$; Czakowska et al. 2000), Mars (quasi-perpendicular; $\theta_p \lesssim 90^\circ$; Treumann & Jaroschek 2008), Jupiter ($\theta_p \simeq 20^\circ$; Gloeckler et al. 2004), Saturn (quasi-perpendicular; interval for different crossings at high angles $60^\circ \lesssim \theta_p \lesssim 100^\circ$; Achilleos et al. 2006, figure 9), Uranus ($\theta_p \simeq 25^\circ$; Bagenal et al. 1987), and Neptune (quasi-perpendicular; $\theta_p \simeq 14^\circ$; Ness et al. 1989; Treumann & Jaroschek 2008). Standoff distances and obstacle curvatures are based on the data-constrained models of Stahara (1984, for Venus, Earth and Mars) and Spreiter & Stahara (1995, for the other planets). Systematic errors on Δ are large, especially for the external and rarely visited planets; in particular, the Δ estimate for Uranus (dashed) is inconclusive (Spreiter & Stahara 1995). For details, assumptions and limitations, see text.

scale extreme, namely the IGM of a galaxy group or cluster. Here, hot bubbles inflated by the active galactic nucleus (AGN) rise buoyantly through the IGM (e.g., Fabian et al. 2000; Nulsen et al. 2005), and the subsonic motion of the plasma in front of them is important, for example, for computing the evolution of the bubbles (e.g., Churazov et al. 2001), and the draping of magnetic fields around them (Lyutikov 2006; Dursi & Pfrommer 2008; Naor & Keshet 2015). Large scale mergers lead to dense clumps moving subsonically or supersonically through the IGM, giving rise to dramatic effects such as shocks, cold fronts, and even a spatial separation between baryonic and dark matter components (Vikhlinin et al. 2001; Markevitch & Vikhlinin 2007). Details such as the bow shock location and the downstream flow pattern are important for correctly interpreting the underlying dynamics.

Consider first a supersonic clump moving through the AGN. A well known example is the 1E0657-56, so-called

bullet, cluster at redshift $z = 0.296$, showing a merger nearly in the plane of the sky (Markevitch et al. 2002; Barrena et al. 2002). The moving clump is seen as a bullet-shaped discontinuity, preceded by a bow shock with $g \simeq 3.0$ (Markevitch 2006) and $\Delta \simeq 2.4 \pm 0.2$. Our analysis indicates that the large Δ corresponds to a weak shock, with $\tilde{M} \simeq 1.1$ (for $\gamma \simeq 5/3$, used henceforth). This is consistent with the $\sim 65^\circ$ asymptotic shock angle far from the nose, which also suggests a $\tilde{M} \simeq 1.1$ shock. However, the high compression ratio corresponds to a much stronger shock with $\tilde{M} \simeq 3$, indicating that the system is not in a steady state. Indeed, plotting the corresponding $\Delta(g)$ on Fig. 2 would suggest an unrealistically soft equation of state. Simulations indicate that the shock velocity can be higher by a factor of 1.7 (Springel & Farrar 2007) or even 6 (Milosavljević et al. 2007) than expected from the clump velocity, because the shock (i) moves faster than the clump; and (ii) plows through gas that is infalling towards the clump (Springel & Farrar 2007). Evidently, Fig. 2 provides a simple way to gauge the relaxation level of a system.

Next consider the subsonic IGM flow in front of an AGN bubble or a slow clump. While previous studies (e.g., Lyutikov 2006; Dursi & Pfrommer 2008) have approximated the motion as incompressible, the inferred velocities are often nearly sonic (Churazov et al. 2001; Markevitch & Vikhlinin 2007), implying considerable compressibility effects. To illustrate this, we compute the magnetization caused by the draping of a weak upstream magnetic field around the moving object. The results are applicable only to weak magnetic fields, where Eqs. (1–2) remain a good approximation.

The magnetic field generally evolves as $\mathbf{B} \propto \rho \mathbf{l}$, where \mathbf{l} is a length element attached to the flow. Hence, the magnetic components initially perpendicular or parallel to the flow evolve along the axis of symmetry according to

$$\frac{B_\perp}{\tilde{B}_\perp} = \left(\frac{\rho/v}{\tilde{\rho}/\tilde{v}} \right)^{1/2} = \left(\frac{M_0}{\tilde{M}_0} \right)^{-1/2} \left(\frac{S^2 - M_0^2}{S^2 - \tilde{M}_0^2} \right)^{S^2/4} \quad (21)$$

or

$$\frac{B_\parallel}{\tilde{B}_\parallel} = \frac{\rho v}{\tilde{\rho} \tilde{v}} = \frac{M_0}{\tilde{M}_0} \left(\frac{S^2 - M_0^2}{S^2 - \tilde{M}_0^2} \right)^{S^2/2}; \quad (22)$$

for a detailed discussion, see Naor & Keshet (2015). The resulting magnetic energy amplification is shown in Fig. 3, for $\gamma = 5/3$, as a function of \tilde{M} and of the normalized distance from the body, $\delta = (r - 1)$. Near the object, the magnetization is predominantly perpendicular, and approximately given by

$$\frac{B_\perp}{\tilde{B}_\perp} \simeq \frac{1 + 1.3\tilde{M}^{2.6}}{3\delta}, \quad (23)$$

as illustrated in the figure.

As the figure shows, the magnetized layer is typically a few times thicker for $\tilde{M} \simeq 1$ than it would appear in the incompressible limit. Such thick layers may have observational implications, through their non-thermal pressure and as synchrotron emission in front of nearly sonic objects. Such a synchrotron signal may contribute to the radio bright edges seen above AGN bubbles, for example in the Virgo cluster (Owen et al. 2000).

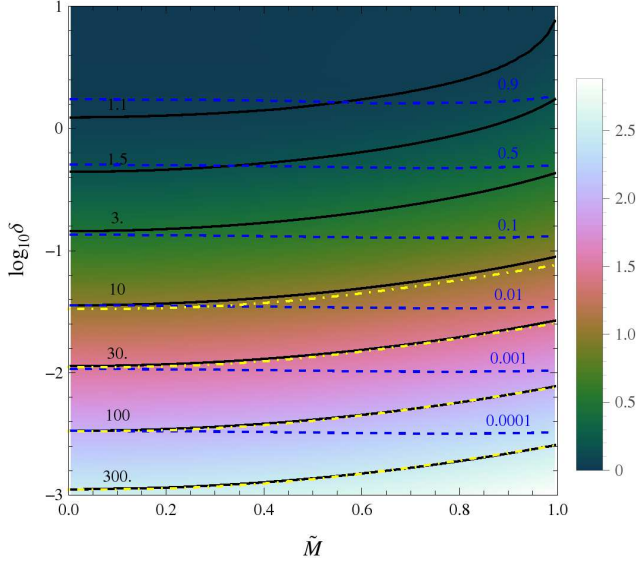


FIG. 3.— Energy amplification of a weak magnetic field initially perpendicular (solid contours, and $\log_{10}(B_{\perp}/B_{\parallel})^2$ cube-helix (Green 2011) colormap) or parallel (dashed contours) to the subsonic $\gamma = 5/3$ flow at a normalized distance $\delta = (r - 1)$ in front of a sphere of Mach number \tilde{M} . Close to the sphere, the field is predominantly perpendicular, and approximately given (dot-dashed contours) by Eq. (23).

6. DISCUSSION

The compressible, inviscid flow in front of a blunt object is approximated analytically, using a hodograph-like, $\mathbf{v} \simeq (-u, q(u)\theta, 0)$ transformation. The velocity (Eq. 7) and pressure (Eq. 4) profiles are derived by expanding q as a (rapidly converging) power series in u (Eq. 8), using the constraints imposed by the object (Eqs. 9 or 10 for a sphere) and by the far upstream subsonic (Eqs. 11–12) or shocked supersonic (Eqs. 14–16) flow. In the latter case, the weak (Eq. 17) and strong shock limits approximately fix the shock curvature (Eq. 18) and consequently the flow, independent of the object shape.

Figure 1 shows that a low order $q(u)$ expansion suffices to recover the measured flow in front of a sphere. The supersonic results also reproduce the measured standoff distance (solid curve and figure inset) of the shock, and constrain its curvature (Eq. 18 or the fit Eq. 19).

Higher-order constraints can be used to improve the approximation further; here we used only the lowest-order constraint at stagnation, and only in the subsonic case.

The axial approximation directly constrains the flow beyond the axis and along the body, as it determines the perpendicular derivatives. For example, one can use it to estimate $\partial_{\theta\theta}P = -\rho_0[q^2 - u\partial_r(rq)](1 - M_0^2/S^2)^{1/(\gamma-1)}$, found by expanding Eqs. (1) to θ^2 order. Extrapolation beyond the axis is simpler in the potential flow regime, where, in particular, $\partial_{\theta\theta}v_r = \partial_r(rq)$.

The axial analysis is generalized for any blunt, axisymmetric object, by modifying the q boundary conditions. For a body with radius of curvature $R_b > 0$ at a stagnation radius r_b , take $\{z \equiv r \cos \theta = R_b - r_b, \varrho \equiv r \sin \theta = 0\}$ as the origin, and rescale lengths by R_b . This maps the stagnation region of the body onto that of the unit sphere, so Eqs. (3–9, 11–16) remain valid. The subsonic analysis is unchanged; for an axisymmetric body, α may need to be altered, *e.g.*, using the Janzen-Rayleigh series. The supersonic analysis is also unchanged, if Eq. (10) is used and adapted for the specific body. The alternative use of Eq. (18) or Eq. (19) is still expected to hold, although higher order terms or a tuned β may be needed if an aspherical body modifies the weak or strong shock limits.

It may be possible to generalize our hodograph-like analysis even for a non-axisymmetric object, using the stagnant streamline instead of the symmetry axis, as long as the corresponding u profile remains monotonic.

Our analysis is applicable to a wide range of subsonic and supersonic astronomical bodies. Illustrative examples are discussed (in §5), on both small, planetary scales, and large, galaxy cluster scales. In particular, plotting the standoff distance as a function of the compression ratio (Fig. 2) can be used to gauge the equation of state and the relaxation level of the system. The results are especially useful for nearly sonic flows, where compressibility effects play an important role; this is seen for example in the thicker magnetically draped layers that form in front of a moving body (Fig. 3), such as a large scale clump or an AGN bubble.

We thank Ephim Golbraikh and Yuri Lyubarsky for helpful advice. This research has received funding from the European Union Seventh Framework Programme (FP7/2007-2013) under grant agreement n° 293975, from an IAEC-UPBC joint research foundation grant, from an ISF-UGC grant, and from an individual ISF grant.

REFERENCES

- Achilleos, N. et al. 2006, *Journal of Geophysical Research (Space Physics)*, 111, 3201
- Allen, J. E. 2013, *Journal of Plasma Physics*, 79, 315
- Anderson, B. J., Acuña, M. H., Korth, H., Purucker, M. E., Johnson, C. L., Slavin, J. A., Solomon, S. C., & McNutt, R. L. 2008, *Science*, 321, 82
- Asanaliev, M. K., Zheebayev, Z. Z., Lelevkin, V. M., Makesheva, K. K., & Pakhomov, E. P. 1988, *Teplofizika Vysokikh Temperatur*, 26, 527
- Aul'chenko, S. M., Zamuraev, V. P., & Kalinina, A. P. 2012, *Journal of Engineering Physics and Thermophysics*, 85, 1372
- Bagenal, F., Belcher, J. W., Sittler, E. C., & Lepping, R. P. 1987, *J. Geophys. Res.*, 92, 8603
- Baker, C. 2010, *Journal of Wind Engineering and Industrial Aerodynamics*, 98, 277
- Baranov, V. B., & Lebedev, M. G. 1988, *APSS*, 147, 69
- Barrena, R., Biviano, A., Ramella, M., Falco, E. E., & Seitz, S. 2002, *A&A*, 386, 816, astro-ph/0202323
- Bono, G., & Awruch, A. M. 2008, *J. of the Braz. Soc. of Mech. Sci. & Eng.*, 189
- Cairns, I. H., & Grabbe, C. L. 1994, *GRL*, 21, 2781
- Canto, J., & Raga, A. 1998, *MNRAS*, 297, 383
- Chapman, J. F., & Cairns, I. H. 2003, *Journal of Geophysical Research (Space Physics)*, 108, 1174
- Churazov, E., Brüggén, M., Kaiser, C. R., Böhringer, H., & Forman, W. 2001, *ApJ*, 554, 261, astro-ph/0008215
- Corona-Romero, P., & Gonzalez-Esparza, A. 2013, *Advances in Space Research*, 51, 1813
- Czaykowska, A., Bauer, T. M., Treumann, R. A., & Baumjohann, W. 2000, *ArXiv Physics e-prints*, physics/0009046

- Dursi, L. J., & Pfrommer, C. 2008, *ApJ*, 677, 993, 0711.0213
- Fabian, A. C. et al. 2000, *MNRAS*, 318, L65, astro-ph/0007456
- Fairfield, D. H., Cairns, I. H., Desch, M. D., Szabo, A., Lazarus, A. J., & Aellig, M. R. 2001, *J. Geophys. Res.*, 106, 25361
- Farris, M. H., & Russell, C. T. 1994, *J. Geophys. Res.*, 99, 17681
- Frank, L. A., Paterson, W. R., Ackerson, K. L., Coroniti, F. V., & Vasyliunas, V. M. 1991, *Science*, 253, 1528
- Gloeckler, G., Geiss, J., & Fisk, L. A. 2004, in *American Institute of Physics Conference Series*, Vol. 719, *Physics of the Outer Heliosphere*, ed. V. Florinski, N. V. Pogorelov, & G. P. Zank, 201–206
- Gollan, R., & Jacobs, P. 2013, *International Journal for Numerical Methods in Fluids*, 73, 19
- Grandemange, M., Gohlke, M., & Cadot, O. 2013, *Journal of Fluid Mechanics*, 722, 51
- . 2014, *Journal of Fluid Mechanics*, 752, 439
- Green, D. A. 2011, *Bulletin of the Astronomical Society of India*, 39, 289, 1108.5083
- Guderley, K. . G. 1962, *The Theory of Transonic Flow*
- Guy, T. B. 1974, *AIAA Journal*, 12, 380
- Hayes, W. D., & Probstein, R. D. 1966, *Dover Publications*, Mineloa, New York
- Heberle, J. W., Wood, G. P., & Gooderum, P. B. 1950, *NACA TECHNICAL NOTE*
- Hejranfar, K., Esfahanian, V., & Najafi, M. 2009, *Journal of Computational Physics*, 228, 3936
- Hida, K. 1953, *Journal of the Physical Society of Japan*, 8, 740
- Hida, K. 1955, *Journal of the Physical Society of Japan*, 10, 882
- Igra, D., & Falcovitz, J. 2010, *Shock Waves*, 20, 441
- Kaplan, C. 1940, *NACA TECHNICAL NOTE*
- Karanjkar, P. V. 2008, PhD thesis, University of Florida
- Kawamura, T. 1950, *Kyoto Univ*, 26, 207
- Krause, E. 1975, *NASA STI/Recon Technical Report N*, 75, 31386
- Landau, L. D., & Lifshitz, E. M. 1959, *Fluid mechanics*
- Lea, S. M., & De Young, D. S. 1976, *ApJ*, 210, 647
- Liepmann, H., & Roshko, A. 1957, *Elements of gasdynamics*
- Lighthill, M. J. 1957, *Journal of Fluid Mechanics*, 2, 1
- Liou, M.-S., & Takayama, K. 2005, *Aerodynamic characteristics of high Mach, low Reynolds numbers flow past micro spheres*, ed. Z. Jiang, 1169
- Lord Rayleigh. 1916, *Phil. Mag.*, ser. 6, 32, 1
- Lytikov, M. 2006, *MNRAS*, 373, 73, astro-ph/0604178
- Mack, C. J., & Schmid, P. J. 2011, *Journal of Fluid Mechanics*, 678, 589
- Markevitch, M. 2006, in *ESA Special Publication*, Vol. 604, *The X-ray Universe 2005*, ed. A. Wilson, 723, astro-ph/0511345
- Markevitch, M., Gonzalez, A. H., David, L., Vikhlinin, A., Murray, S., Forman, W., Jones, C., & Tucker, W. 2002, *ApJ*, 567, L27, astro-ph/0110468
- Markevitch, M., & Vikhlinin, A. 2007, *Phys. Rep.*, 443, 1, astro-ph/0701821
- Marrone, S., Colagrossi, A., Antuono, M., Colicchio, G., & Graziani, G. 2013, *Journal of Computational Physics*, 245, 456
- Milosavljević, M., Koda, J., Nagai, D., Nakar, E., & Shapiro, P. R. 2007, *ApJ*, 661, L131, astro-ph/0703199
- Moeckel, W. E. 1949, *NACA TECHNICAL NOTE*
- Nakanishi, Y., & Kamemoto, K. 1993, *Journal of Wind Engineering and Industrial Aerodynamics*, 46, 363
- Naor, Y., & Keshet, U. 2015, *ArXiv e-prints*, 1501.06892
- Ness, N. F., Acuna, M. H., Burlaga, L. F., Connerney, J. E. P., & Lepping, R. P. 1989, *Science*, 246, 1473
- Nulsen, P. E. J., McNamara, B. R., Wise, M. W., & David, L. P. 2005, *ApJ*, 628, 629, astro-ph/0408315
- Owen, F. N., Eilek, J. A., & Kassim, N. E. 2000, *ApJ*, 543, 611, astro-ph/0006150
- Park, H., Lee, D., Jeon, W.-P., Hahn, S., Kim, J., Kim, J., Choi, J., & Choi, H. 2006, *Journal of Fluid Mechanics*, 563, 389
- Petrinec, S. M. 2002, *Planetary and Space Science*, 50, 541
- Petrinec, S. M., & Russell, C. T. 1997, *Advances in Space Research*, 20, 743
- Pilyugin, N. N., & Khlebnikov, V. S. 2006, *Fluid Dynamics*, 41, 483
- Schulreich, M. M., & Breitschwerdt, D. 2011, *A&A*, 531, A13, 1104.4701
- Schwartz, R. N., & Eckerman, J. 1956, *Journal of Applied Physics*, 27, 169
- Sedney, R., & Kahl, G. D. 1961, *Planet. Space Sci.*, 4, 337
- Shaviv, G., & Salpeter, E. E. 1982, *A&A*, 110, 300
- Slavin, J. A. et al. 2012, *Journal of Geophysical Research (Space Physics)*, 117, 1215
- Spreiter, J. R., & Alksne, A. Y. 1970, *Annual Review of Fluid Mechanics*, 2, 313
- Spreiter, J. R., & Stahara, S. S. 1995, *Advances in Space Research*, 15, 433
- Spreiter, J. R., Summers, A. L., & Alksne, A. Y. 1966, *Planet. Space Sci.*, 14, 223
- Springel, V., & Farrar, G. R. 2007, *MNRAS*, 380, 911, astro-ph/0703232
- Stahara, S. S. 1984, *NASA STI/Recon Technical Report N*, 84, 26510
- Stangeby, P. C., & Allen, J. E. 1971, *Journal of Plasma Physics*, 6, 19
- Tamada, K. 1939, *Proe. Phys-Math. Soc., Japan*, 21, 743
- Treumann, R. A., & Jaroschek, C. H. 2008, *ArXiv e-prints*, 0808.1701
- Tutty, O. R., Roberts, G. T., & Schuricht, P. H. 2013, *Journal of Fluid Mechanics*, 737, 19
- Van Dyke, M. D. 1958a, *Journal of Fluid Mechanics*, 3, 515
- Van Dyke, M. D. 1958b, *Journal of Aeronautical Sciences*, 25, 485
- . 1975, *Perturbation methods in fluid dynamics (Parabolic Press)*
- Verigin, M. et al. 2003, *Journal of Geophysical Research (Space Physics)*, 108, 1323
- Verigin, M. I. et al. 1999, *Kosmicheskie Issledovaniia*, 37, 38
- Vikhlinin, A., Markevitch, M., & Murray, S. S. 2001, *ApJ*, 551, 160, astro-ph/0008496
- Volkov, A. N. 2009, *Fluid Dynamics*, 44, 141
- Wilson, H. J. 2013, *Journal of Computational Physics*, 245, 302

APPENDIX

A. EXPLICIT DESCRIPTION OF THE AXIAL FLOW

Here we present the flow in front of a sphere in explicit form, for both subsonic and supersonic regimes. Fully analytic expressions are provided to second order in the supersonic case, and to third order in the subsonic case. The generalization to an arbitrary axisymmetric blunt object is discussed in §6.

A.1. Subsonic regime

In the subsonic regime, $q(u)$ is constrained at stagnation and at infinity; we may expand it equivalently either around the stagnation point ($u = 0$) or around infinity ($u = \tilde{u}$). Here we arbitrarily choose to write $q(u)$ using an expansion at stagnation, namely

$$q = \bar{q}_0 - \frac{1}{2}u + \bar{q}_3u^3 + O(u^4), \quad (\text{A1})$$

where we used the stagnation boundary conditions $\bar{q}_1 = (-1/2)$ and $\bar{q}_2 \simeq 0$ derived in the main text. This expression is matched with the boundary conditions at $r \rightarrow \infty$, in order to find the remaining coefficients,

$$\bar{q}_0 = \frac{3}{2}\tilde{u} - \bar{q}_3\tilde{u}^3 \quad \text{and} \quad \bar{q}_3 = \frac{(S/W)^2 - 1}{2(S^2\bar{c}^2 - \tilde{u}^2)}. \quad (\text{A2})$$

A.2. Supersonic regime

In the supersonic regime, we may write $q(u)$ using the downstream expansion at the shock,

$$q = q_0^{(d)} + q_1^{(d)}(u - u_d) + q_2^{(d)}(u - u_d)^2, \quad (\text{A3})$$

where the coefficients are given in the main text.

A.3. Explicit analytic results

By plugging the relevant expressions for $q(u)$ into Eq. (7), $r(u)$ can be computed in both subsonic and supersonic cases. In the latter, the shock radius is then determined as $r_s = 1 + \Delta = r(u_d)$. The integral in Eq. (7) is easily evaluated numerically, using either Eq. (A1) or (A3) for q . However, the integral can also be carried out analytically, as follows.

A.3.1. Subsonic regime

In the subsonic case, plugging $q(u)$ from Eq. (A1) into Eq. (7), and carrying out the integral, yields

$$\ln(r) = \frac{S^2}{2W^2} \frac{\bar{c}(S^2 - W^2) \left(\frac{1}{2}\bar{c} \left(\frac{3}{2} - S^2\bar{c}^2\bar{q}_3 \right) \ln \left(1 - \frac{u^2}{S^2\bar{c}^2} \right) - \frac{\bar{q}_0}{S} \coth^{-1} \left(\frac{S\bar{c}}{u} \right) \right) - F(u) + F(0)}{\bar{q}_0^2 - S^2\bar{c}^2 \left(S^2\bar{c}^2\bar{q}_3 - \frac{3}{2} \right)^2}, \quad (\text{A4})$$

where we defined

$$F(u) \equiv H \left[x^3\bar{q}_3 + \bar{q}_0 - \frac{3x}{2}, \right. \\ \left. \frac{\ln(u-x) \left(\bar{c}^2 (2S^2\bar{c}^2\bar{q}_3 - 3) (W^2 (2\bar{q}_3 (S^2\bar{c}^2 + x^2) - 3) - 2S^2x^2\bar{q}_3) + 4x\bar{c}^2\bar{q}_0\bar{q}_3 (S^2 - W^2) - 4\bar{q}_0^2 \right)}{12x^2\bar{q}_3 - 6} \right], \quad (\text{A5})$$

and $H(a, b)$ is the root sum function, giving the sum of $b(x)$ over all roots x of $a(x)$.

A.3.2. Supersonic regime

For the supersonic regime, the same procedure using Eq. (A3) yields

$$\ln(r) = \frac{S^2}{2W^2} \frac{\bar{c}(S^2 - W^2) \left(\bar{c} (q_2u_d - \frac{q_1-1}{2}) \ln \left(1 - \frac{u^2}{S^2\bar{c}^2} \right) + \frac{\coth^{-1}(\frac{S\bar{c}}{u})(q_1u_d - q_2S^2\bar{c}^2 - q_2u_d^2 - q_0)}{S} \right) + G(u) - G(0)}{(q_2S^2\bar{c}^2 + u_d(q_2u_d - q_1) + q_0)^2 - S^2\bar{c}^2(2q_2u_d - q_1 + 1)^2}, \quad (\text{A6})$$

where we omitted the (d) superscripts on the coefficients q , and defined

$$G(u) \equiv H \left\{ q_2(u_d - x)^2 + q_1(x - u_d) + q_0 - x, \right. \\ \left. \frac{\ln(u-x)}{2q_2(x - u_d) + q_1 - 1} \left[q_0(q_2\bar{c}^2(S^2 + W^2) + 2u_d(q_2u_d - q_1)) + q_2^2S^2W^2\bar{c}^4 + u_d^2(q_1 - q_2u_d)^2 + q_0^2 \right. \right. \\ \left. \left. + \bar{c}^2(q_2x(S^2 - W^2)(-2q_2u_d + q_1 - 1) + q_2S^2u_d(q_2u_d - q_1) + W^2(-3q_2^2u_d^2 + (3q_1 - 4)q_2u_d - (q_1 - 1)^2)) \right] \right\}. \quad (\text{A7})$$

A.3.3. Shock standoff distance

The standoff distance Δ may be found by computing $r_s = (1 + \Delta)$ from Eq. (A6) with $u = u_d$. In the strong shock limit, the downstream Mach number is given by $M_0 = S/g = W^2/S$, and one obtains (after considerable algebra)

$$r_s = \gamma^{G+} [4(2 + \gamma + \gamma^{-1})]^{G-} A_-^{B-} A_+^{B+}, \quad (\text{A8})$$

where

$$A_{\pm} \equiv \frac{\gamma(\gamma(5\gamma-6)-3\pm C)}{4+\gamma(\gamma(-37+\gamma(19+5\gamma))-15\pm 4C)}, \quad (\text{A9})$$

$$B_{\pm} \equiv \frac{(-1+\gamma)(\pm 40-2C(-1+\gamma)(4+\gamma(-15+\gamma(-37+\gamma(19+5\gamma)))) \pm \gamma(-266+\gamma(529+\gamma(27+\gamma(-174+\gamma(-292+7\gamma(19+5\gamma))))))}{C(32+\gamma(5+\gamma)(-11+5\gamma))(4+\gamma(-19+\gamma(10+\gamma)))}, \quad (\text{A10})$$

$$C \equiv \sqrt{\gamma(\gamma(5\gamma - 56) + 58) + 48} - 7, \quad (\text{A11})$$

and

$$G_{\pm} \equiv -2 \pm \frac{2-2\gamma}{32+\gamma(5+\gamma)(-11+5\gamma)} + \frac{8-38\gamma+22\gamma^2}{4+\gamma(-19+\gamma(10+\gamma))}. \quad (\text{A12})$$

This roughly gives $\Delta \sim 2/(3g)$. Other fits in the range $1 < \gamma < 2$ include $\Delta \simeq 0.61g^{-0.94}$ and $\Delta \simeq 0.37(g-1)^{-0.75}$.